

Transmission gaps from corrugations

Yong-Long Wang^{1,2,*}, Guo-Hua Liang¹, Hua Jiang^{1,2}, Wei-Tao Lu², and Hong-Shi Zong^{1,3,4†}

¹ *Department of Physics, Nanjing University, Nanjing 210093, P. R. China*

² *School of Science and Institute of Condensed Matter Physics, Linyi University, Linyi 276005, P. R. China*

³ *Joint Center for Particle, Nuclear Physics and Cosmology, Nanjing 210093, P. R. China and*

⁴ *State Key Laboratory of Theoretical Physics, Institute of Theoretical Physics, CAS, Beijing 100190, P. R. China*

A model including a periodically corrugated thin layer with GaAs substrate is employed to investigate the effects of the corrugations on the transmission probability of the nanostructure. We find that transmission gaps and resonant tunneling domains emerge from the corrugations, in the tunneling domains the tunneling peaks and valleys result from the boundaries between adjacent regions in which electron has different effective masses, and can be slightly modified by the layer thickness. These results can provide an access to design a curvature-tunable filter.

PACS Numbers: 73.50.-h, 73.20.-r, 03.65.-w, 02.40.-k

I. INTRODUCTION

With the advent and development of nanostructure technology, a variety of nanostructures with complex geometries were successfully fabricated, such as corrugated semiconductor films^{1–6}, rolled-up nanotubes^{7–12}, Möbius stripes^{13–15}, peanut-shaped C_{60} polymers^{16–20}. These successes in experiment found the basis of the emerging nanoelectronics. In the two-dimensional (2D) reduced systems, the dynamics of confined electron is affected by the surface curvature. As an important consequence, the geometric potential induced by the curvature appears in the effective surface quantum equation^{21–24} by the thin-layer quantization procedure^{25–28}. In the procedure, a squeezing potential is introduced to accomplish the reduction of the number of the spatial variables of the curved systems. Physically, the squeezing process is probably severe and breaks with the natural limits set by the uncertainty principle. Even so, the present quantization scheme can be safely applied to study the motion of confined electron when the quantum excitation energies in the normal direction are raised far beyond those in the tangential direction. Actually, the thin-layer quantization method has successfully been employed to calculate the band-structure of real systems^{29–31}, determine the localized surface states in geometrically deformed quantum systems^{32–38}, and study the transport properties of electron confined in the systems with complex geometries^{39–42}. Furthermore, the experimental evidences for the geometrical effects of the curved surface have been presented, such as the realization of an optical analog of the curvature-induced geometric potential⁴³, the observation of the influence of geometry on proximity effect⁴⁴ and the observation of Riemannian geometrical effects on electronic states¹⁹. In other words, the geometrical deformation can be concluded as the presence of geometric potential in the dimensionally reduced quantum equation.

In the same vein, the advent and development of nanostructures have clearly led to a frontier field in 2D semiconductor research^{45–50}. It is now possible to design and

fabricate materials with prescribed electronic and photonic properties by artificial band-gap engineering. In order to satisfy the requirement of the development of nanoelectronics, theoretical physicists have tried to study the effects of the geometrical deformation on the tunneling rate⁵¹, the electrical resistivity^{52,53} and the persistent current^{54,55}. Moreover, on the basis of the geometric potential, quantum-electromechanical circuits^{56–58} and thin film transistors⁵⁹ have been proposed.

In fact, over the years, the electronic properties of the periodically curved surface have been the subject of active studies, both theoretical and experimental, due to the demand in understanding the physics involved and its great application potential. The ability to confine electron nearly to 2D regions on nanostructures has given a new impetus toward understanding the physics of reduced dimensionality systems. An important property of nanostructures is how their geometries affect their behaviors. Usually, one thinks of geometrical effects being connected primarily with the physical size and barrier configuration that define the confining region of the nanostructure.

In the present study, we consider a model⁵¹ (shown in Fig. 1) which contains two barriers and a well, the well is fabricated as a periodically corrugated thin layer. In the model, R_1 denotes free electron beam source, R_2 is a barrier with width $d = 1\text{\AA}$, R_3 is a corrugated thin layer with width $L = 1000\text{\AA}$, R_4 is the other barrier with width $d = 1\text{\AA}$, and R_5 denotes a drain, from left to right. The

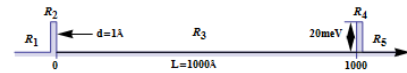


FIG. 1. (Color online) Model nanostructure schematic configuration parameters used to investigate the effects of the layer curvature and thickness on transmission probability.

double barriers resonant tunneling structure is a typical microstructure that has been the focus of many investigations^{60–65}. In the present model, the corrugations are employed to provide transmission gaps and resonant tunneling domains, the double barriers and the boundaries

between adjacent regions, in which electron has different effective masses, are adopted to generate the tunneling peaks and valleys in the tunneling domains. The theoretical basis is that when the spatial dimension is reduced to a scale being comparable with the de Broglie wavelength of electron in the vicinity of Fermi energy in the model, the wave nature of electron is expected to play an increasingly important role in transport properties.

This paper is organized as follows. In Sec. II, we briefly review the effective quantum equation for electron confined in a periodically corrugated layer by the thin-layer quantization scheme, and analyze the curvature-induced geometric potential. In Sec. III, we obtain a new geometric potential by the extended thin-layer quantization scheme, and also analyze the thickness-modified geometric potential. In Sec. IV, we investigate the effects of the corrugations, double barriers and boundaries on transmission probability. Finally in Sec. V the conclusions are given.

II. QUANTUM DYNAMICS OF A PARTICLE CONFINED ON A PERIODICALLY CORRUGATED SURFACE

A 2D curved surface S embedded in the usual three-dimensional (3D) space can be parametrized by $\vec{r} = \vec{r}(q_1, q_2)$, where q_1 and q_2 are the curvilinear coordinate variables over S . With respect to q_1 and q_2 , two unit basis vectors \vec{e}_1 and \vec{e}_2 over S are defined by $\vec{e}_1 = \frac{\partial \vec{r}}{\partial q_1} / |\frac{\partial \vec{r}}{\partial q_1}|$ and $\vec{e}_2 = \frac{\partial \vec{r}}{\partial q_2} / |\frac{\partial \vec{r}}{\partial q_2}|$, respectively. By introducing a curvilinear coordinate variable q_3 along the direction normal to S , a 3D subspace V_N consisting of points near to S and on S can be described by $\vec{R}(q_1, q_2, q_3) = \vec{r}(q_1, q_2) + q_3 \vec{e}_n(q_1, q_2)$, where $\vec{e}_n(q_1, q_2)$ is the unit basis vector perpendicular to S , with the definition $\vec{e}_n = (\vec{e}_1 \times \vec{e}_2) / (|\vec{e}_1 \times \vec{e}_2|)$. In V_N , the covariant components of the metric tensor are defined by $G_{ij} = \frac{\partial \vec{R}}{\partial q^i} \cdot \frac{\partial \vec{R}}{\partial q^j}$ ($i, j = 1, 2, 3$). On S , the covariant components of the reduced metric tensor are determined by $g_{ab} = \frac{\partial \vec{r}}{\partial q^a} \cdot \frac{\partial \vec{r}}{\partial q^b}$ ($a, b = 1, 2$). The relationships between G_{ab} and g_{ab} are

$$G_{ab} = g_{ab} + (\alpha g + g^T \alpha^T)_{ab} q_3 + (\alpha g \alpha^T)_{ab} (q_3)^2, \quad (1)$$

and $G_{a3} = G_{3a} = 0$, $G_{33} = 1$, where T denotes the matrix transpose, α is the Weingarten curvature matrix

$$\alpha = \frac{1}{g} \begin{pmatrix} g_{12}h_{21} - g_{22}h_{11} & g_{21}h_{11} - g_{11}h_{21} \\ g_{12}h_{22} - g_{22}h_{12} & g_{12}h_{21} - g_{11}h_{22} \end{pmatrix}, \quad (2)$$

wherein h_{ab} are the coefficients of the second fundamental form, $h_{ab} = \vec{e}_n \cdot \frac{\partial^2 \vec{r}}{\partial q^a \partial q^b}$. By means of α , the mean curvature M is $M = \frac{1}{2} \text{Tr}(\alpha)$ and the Gaussian curvature $K = \det(\alpha)$, and then the relation between $G = \det(G_{ij})$ and $g = \det(g_{ab})$ is $G = f^2 g$ with $f = 1 + 2Mq_3 + K(q_3)^2$.

Basing on the above mathematical formula, we can confine a free electron on a curved surface by the

thin-layer quantization scheme^{25,26}, the effective surface Schrödinger equation is obtained as

$$-\frac{\hbar^2}{2m} \frac{1}{\sqrt{g}} \partial_a (\sqrt{g} g^{ab} \partial_b \chi_s) + V_g \chi_s = E_s \chi_s, \quad (3)$$

where V_g is the geometric potential

$$V_g = -\frac{\hbar^2}{2m} (M^2 - K). \quad (4)$$

Practically, nanocorrugated thin-films are often found in nanomaterial experiments. For the sake of simplicity, a curved surface S shown in Fig. 2 is considered. It is corrugated along the direction of x with period $2\pi/\gamma$, amplitude a , but is flat along that of y . In the Monge form, S can be described as

$$\vec{r} = \vec{e}_x x + \vec{e}_y y + \vec{e}_z a \cos(\gamma x). \quad (5)$$

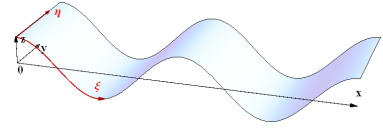


FIG. 2. (Color online) Schematic of a periodically corrugated surface described by $z = a \cos(\gamma x)$. Here a and $2\pi/\gamma$ are the amplitude and period length of the corrugations, respectively. (ξ, η) denotes the two curvilinear coordinates over surface.

According to the procedure mentioned above, from Eq. (5) we obtain three unit basis vectors and corresponding three derivative elements

$$\begin{aligned} \vec{e}_\xi &= w \vec{e}_x + w a \gamma \sin(\gamma x) \vec{e}_z, & d\xi &= \frac{1}{w} dx, \\ \vec{e}_\eta &= \vec{e}_y, & d\eta &= dy, \\ \vec{e}_n &= -w a \gamma \sin(\gamma x) \vec{e}_x + w \vec{e}_z, & dq_3 &= dq_3, \end{aligned} \quad (6)$$

respectively, with

$$w = \frac{1}{\sqrt{1 + a^2 \gamma^2 \sin^2(\gamma x)}}. \quad (7)$$

Subsequently, we obtain (G_{ab}) and G

$$(G_{ab}) = \begin{pmatrix} (1 + q_3 k)^2 & 0 \\ 0 & 1 \end{pmatrix}, \quad G = (1 + q_3 k)^2, \quad (8)$$

the Weingarten curvature matrix α

$$\alpha = \begin{pmatrix} k & 0 \\ 0 & 0 \end{pmatrix}, \quad (9)$$

(g_{ab}) and g

$$(g_{ab}) = \begin{pmatrix} 1 & 0 \\ 0 & 1 \end{pmatrix}, \quad g = 1, \quad (10)$$

where $k = w^3 a \gamma^2 \cos(\gamma x)$. In the above calculated process, the factor f , the mean curvature M and the Gaussian curvature K can be given as

$$f = 1 + kq_3, \quad M = \frac{1}{2}k, \quad K = 0. \quad (11)$$

Consequently, the expected Schrödinger equation (3) is

$$-\frac{\hbar^2}{2m^*} \left[w \frac{\partial}{\partial x} \left(w \frac{\partial}{\partial x} \right) + \frac{\partial^2}{\partial y^2} \right] \chi_s + V_g \chi_s = E_s \chi_s, \quad (12)$$

where m^* denotes the effective mass of electron, and V_g is the geometric potential

$$V_g = -\frac{\hbar^2}{8m^*} \frac{[a\gamma^2 \cos(\gamma x)]^2}{[1 + a^2\gamma^2 \sin^2(\gamma x)]^3}. \quad (13)$$

These results are the same as those given by S. Ono and H. Shima⁵². The quantum motion in the normal direction is neglected, because the introduced squeezing potential raises the quantum excitation energies in normal direction far beyond those in tangential direction^{25,26}.

As the central result of the thin-layer quantization scheme, the geometric potential appears in the expectant quantum equation. With $n = 3$ and $m^* = 0.067m_0$ ($0.067m_0$ is the effective mass of electron in GaAs substrate) the geometric potential $V_g(x)$ shown in Fig. 3 is a function of γx and a , where n denotes the period number of the corrugations in R_3 , m_0 is the mass of a free electron. As observed in Fig. 3 (a), the x dependence of $V_g(x)$ deviates considerably from a cosinusoidal surface, whereas the surface corrugation is exactly cosinusoidal. It is shown in Fig. 3 (b) that the downward peaks are formed at $\gamma x = \pm l\pi$ ($l = 0, 1, 2, \dots$), here the height of the surface \mathcal{S} is either maximum ($z = a$) or minimum ($z = -a$). The amplitude of the peaks grows sharply with increasing a that is highlighted in Figs. 3 (b) and (c). As a consequence, we can provide a list of attractive potential wells by introducing corrugations, tune their depths by a , and design their number by n .

III. THE MODIFICATION OF THE LAYER THICKNESS TO THE GEOMETRIC POTENTIAL

Really, the corrugated layer has certain thickness. The thickness effects on the effective quantum equation (12) can be investigated by the extended thin-layer quantization scheme²⁸. In the present model the thickness effects on the kinetic term can be neglected, because the thickness lengthens the displacement of electron across the layer very slightly, whereas a thickness-modified geometric potential V'_g can be given as

$$V'_g = V_g + \frac{\hbar^2}{4m^*} \frac{[a\gamma^2 \cos(\gamma x)]^3}{[1 + a^2\gamma^2 \sin^2(\gamma x)]^{\frac{9}{2}}} h, \quad (14)$$

where h denotes the layer thickness sketched in Fig. 4 and V_g is the geometric potential (13). The second term

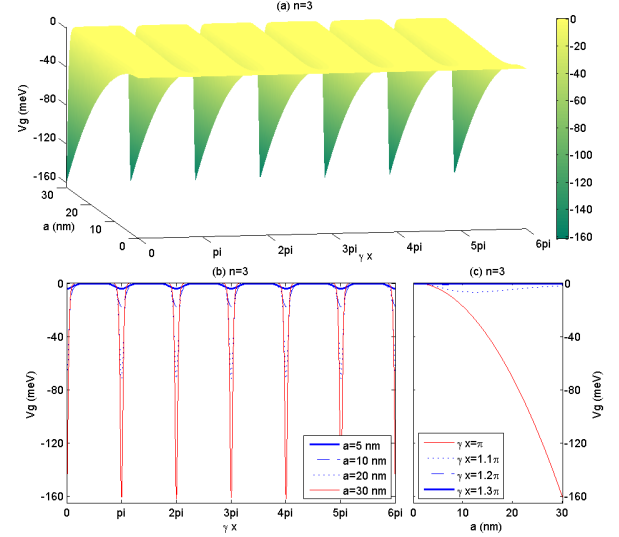


FIG. 3. (Color online) (a) Surface of V_g with $n = 3$, as a function of γx and a . (b) Slices of the geometric potential V_g at $a = 5\text{nm}, 10\text{nm}, 20\text{nm}, 30\text{nm}$, as a function of γx . (c) Slices of the geometric potential V_g at $\gamma x = \pi, 1.1\pi, 1.2\pi, 1.3\pi$, as a function of a .

on the right hand side of Eq. (14) attributes to the layer thickness. It needs to notice that h must be less than the minimum curvature radius on \mathcal{S} . For an arbitrary point on \mathcal{S} , there is only one principle curvature $k = w^3 a \gamma^2 \cos(\gamma x)$, the corresponding curvature radius is

$$\rho = \frac{[1 + a^2\gamma^2 \sin^2(\gamma x)]^{\frac{3}{2}}}{a\gamma^2 \cos(\gamma x)}. \quad (15)$$

It is obvious that the minimum curvature radius is $\rho_{\min} = 1/(a\gamma^2)$ at $\gamma x = n\pi$ ($n = 0, \pm 1, \pm 2, \dots$). When $h = \rho_{\min}$, at new points (they have a uniform distance ρ_{\min} to \mathcal{S}) " $h - \rho_{\min}$ " is 0, the corresponding mean curvature M becomes ∞ . In order to avoid the trouble, we primitively define h ranging between 0 and $1/(2a\gamma^2)$.

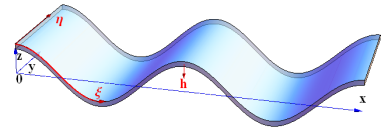


FIG. 4. (Color online) Schematic of a periodically curved layer with a uniform thickness h . The standard surface of the layer is described by $z = a \cos(\gamma x)$. Here a and $2\pi/\gamma$ are the amplitude and period length of corrugations, respectively. (ξ, η) are the two curvilinear coordinates over layer.

As an important result for the extended thin-layer quantization scheme²⁸, the modification of the layer thickness is included in $V'_g(x)$, as a function of γx and h , described in Fig. 5 with $n = 3$ and $a = 12\text{nm}$. As mentioned above, the downward peaks are still formed

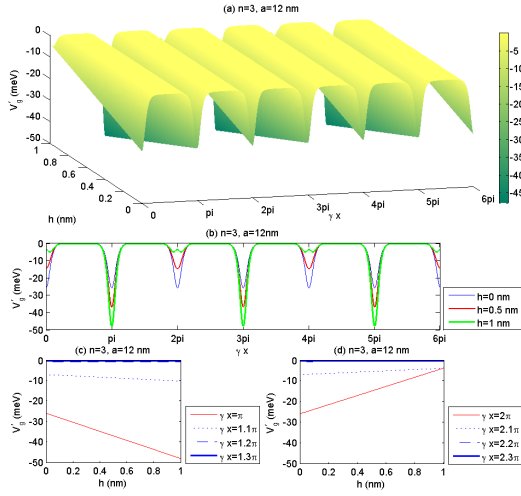


FIG. 5. (Color online) (a) Surface of V'_g with $n = 3$ and $a = 12nm$, as a function of γx and h . (b) Slices of V'_g at $h = 0nm, 0.5nm, 1nm$, as a function of γx with $n = 3$ and $a = 12nm$. (c) Slices of V'_g at $\gamma x = \pi, 1.1\pi, 1.2\pi, 1.3\pi$, as a function of h with $n = 3$ and $a = 12nm$. (d) Slices of V'_g at $\gamma x = 2\pi, 2.1\pi, 2.2\pi, 2.3\pi$, as a function of h .

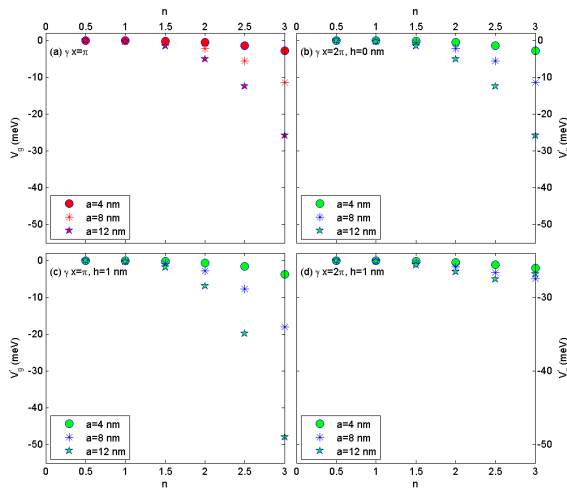


FIG. 6. (Color online) (a) The downward peaks of V_g at $\gamma x = \pi$ versus n for $a = 4nm, 8nm, 12nm$. (b) The downward peaks of V'_g at $\gamma x = 2\pi$ and $h = 0nm$ versus n for $a = 4nm, 8nm, 12nm$. (c) The downward peaks of V'_g at $\gamma x = \pi$ and $h = 1nm$ versus n for $a = 4nm, 8nm, 12nm$. (d) The downward peaks of V'_g at $\gamma x = 2\pi$ and $h = 1nm$ versus n for $a = 4nm, 8nm, 12nm$.

at $\gamma x = \pm l\pi$ ($l = 0, 1, 2, \dots$). However, there is a change shown in Fig. 5 (a), the downward peaks at $\gamma x = \pm(2m+1)\pi$ ($m = 0, 1, 2, \dots$) grow with increasing h , but those at $\gamma x = \pm 2m\pi$ dwarf, that is highlighted in Figs. 5 (b), (c) and (d).

The scales of $V_g(x)$ and $V'_g(x)$ are substantially influenced by n described in Figs. 6 (a) and (b), the larger the period number n , the deeper the peaks at $\gamma x = l\pi$ ($l = 0, 1, 2, \dots$). Obviously, as shown in Figs. 6 (c) and (d), h evidently deepens the peaks at $\gamma x = (2l+1)\pi$, but

remarkably shallows those at $\gamma x = 2l\pi$. In other words, we can adjust the discrepancy between adjacent wells by depositing the layer thickness h finely.

IV. TRANSMISSION PROBABILITY IN THE PERIODICALLY CORRUGATED THIN LAYER

A. Transmission probability

According to Eq. (12), with the limit $h \rightarrow 0$ the quantum equation for an electron in the model depicted in Fig. 1 can be

$$-\frac{\hbar^2}{2m^*}w\frac{d}{dx}\left[w\frac{d}{dx}\psi(x)\right] + V(x)\psi(x) = E\psi(x), \quad (16)$$

where $m^* = 0.067m_0$ (the effective mass of electron in GaAs substrate) if $x \in R_3$ and $m^* = m_0$ otherwise, $w = 1/\sqrt{1 + a^2\gamma^2 \sin^2(\gamma x)}$ if $x \in R_3$ and $w = 1$ otherwise, ψ is a wave function, E is the energy with respect to ψ and $V(x)$ is

$$V(x) = \begin{cases} 0meV, & x \in R_1, \\ 20meV, & x \in R_2, \\ V_g(x), & x \in R_3, \\ 20meV, & x \in R_4, \\ 0meV, & x \in R_5, \end{cases} \quad (17)$$

wherein $V_g(x)$ is the geometric potential (13) and meV denotes milli electron volts. When the effects of the layer thickness are considered, $V_g(x)$ should be replaced by $V'_g(x)$ in Eq. (14).

With the help of the transfer matrix technique⁶⁶, instead of dealing with continuous variations of $V(x)$ in R_3 , we split R_3 up into segments, in each segment $V(x)$ can be regarded as a constant. And then let us assume R_3 will be a sequence N_3 small segments, R_2 one segment ($N_2 = 1$) and R_4 one segment ($N_4 = 1$). It is straightforward to obtain that the total number of segments is $N = N_2 + N_3 + N_4$, that of boundaries is $N + 1$. For an arbitrary segment, the j th region, in which the wave function $\psi_j(x)$ can be given by

$$\psi_j(x) = A_j \exp[ik_j \xi(x)] + B_j \exp[-ik_j \xi(x)], \quad (18)$$

where

$$k_j = \frac{\sqrt{[2m_j^*(E - U_j)]}}{\hbar}, \quad (19)$$

wherein \hbar is the reduced Planck's constant, m_j^* is the effective mass for electron at the middle point in the j th region, U_j is a constant, $U_j = V(\frac{x_{j-1}+x_j}{2})$. For the wave function (18), it is particular that the curvilinear coordinate variable $\xi(x)$ as a function of x has the derivative form $d\xi = \sqrt{1 + a^2\gamma^2 \sin^2(\gamma x)}dx$ if $x \in R_3$ and $d\xi = dx$ otherwise.

On account of the continuities of $\psi_j(x)$ and $\psi'_j(x)/m_j^*$ at each boundary, we can determine A_j and B_j in Eq. (18) by the following multiplication

$$\begin{pmatrix} A_j \\ B_j \end{pmatrix} = \prod_{l=0}^{j-1} M_l \begin{pmatrix} A_0 \\ B_0 \end{pmatrix}, \quad (20)$$

$$M_l = \frac{1}{2} \begin{bmatrix} (1 + s_l) \exp[-i(k_{l+1} - k_l)x_l] & (1 - s_l) \exp[-i(k_{l+1} + k_l)x_l] \\ (1 - s_l) \exp[i(k_{l+1} + k_l)x_l] & (1 + s_l) \exp[i(k_{l+1} - k_l)x_l] \end{bmatrix} \quad (21)$$

with

$$s_l = \frac{m_{l+1}^*}{m_l^*} \frac{k_l}{k_{l+1}}. \quad (22)$$

As $j = N$, the equation (20) becomes

$$\begin{pmatrix} A_N \\ B_N \end{pmatrix} = M \begin{pmatrix} A_0 \\ B_0 \end{pmatrix}, \quad (23)$$

where

$$M = \begin{pmatrix} M_{11} & M_{12} \\ M_{21} & M_{22} \end{pmatrix} = \prod_{l=1}^N M_l. \quad (24)$$

Without any loss of generality, we assume that in the model under study R_1 is an electron source consisting of free electrons, and R_5 is a drain. Using the plane wave approximation, the wave function in R_1 can be

$$\psi_0(x) = \exp(ik_0x_0) + B_0 \exp(-ik_0x_0), \quad (25)$$

and in R_5

$$\psi_N(x) = A_N \exp(ik_Nx_N), \quad (26)$$

where B_0 and A_N are the coefficients of reflection and transmission, respectively. In the case of $A_0 = 1$, $B_N = 0$, $m_0^* = m_{N+1}^* = m_0$ and $k_0 = k_{N+1}$, we can obtain the transmission amplitude A_N and the transmission probability T as

$$A_N = \frac{1}{M_{22}}, \quad (27)$$

and

$$T = \frac{1}{(M_{22})^2}, \quad (28)$$

respectively.

B. Numerical results and analysis

In this subsection, we will investigate how the corrugations affect the transmission probability by the transfer matrix method. Before beginning the investigation,

where

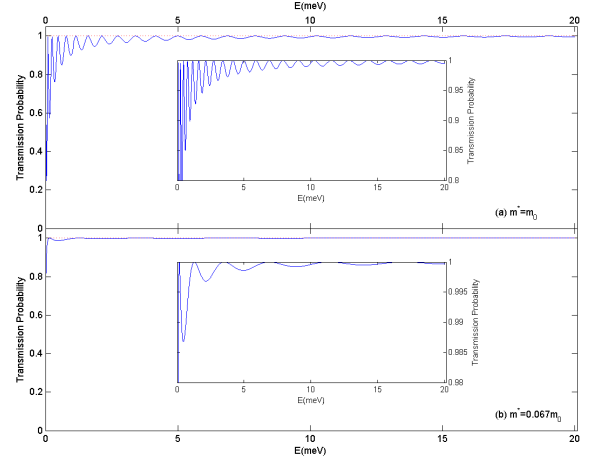


FIG. 7. (Color online) Transmission probability versus incident energy E for the model with $V(x) = 20\text{meV}$ in R_2 and R_4 , $V(x) = 0\text{meV}$ otherwise, and m^* for (a) $m^* = m_0$ and (b) $m^* = 0.067m_0$.

we briefly analyze the effects of other components in the model on the transmission probability. The effective masses of electron in the model are closely related to the resonant tunneling peaks as shown in Figs. 7. When the effective mass is less, the number of the peaks is less, their amplitudes smaller. These results are highlighted in the insets in Fig. 7.

In the case of the model with $m^* = 0.067m_0$ in R_3 and $m^* = m_0$ otherwise, the two boundaries between R_2 and R_3 , R_3 and R_4 are essential to influence the transmission probability. In response to the boundaries, the amplitudes of the tunneling peaks considerably grow shown in Fig. 8. In other words, these peaks are mostly provided by the continuities of $\psi(x)$ and $\psi'(x)/m^*$, the contributions of the double barriers could be neglected. It is worth noticing that the peaks almost reach 1, the valleys are about 0.235. Physically, the peaks occur when the length of R_3 strictly equals integer multiple times of a half wave length of electron, the bottom of the valleys is eventually determined by the ratio of the effective masses in R_3 and R_2 (or R_4).

In a special case, the model without the double barriers, with $m^* = 0.067m_0$ in all regions, $V(x) = V_g(x)$ in R_3 and $V(x) = 0\text{meV}$ otherwise, transmission

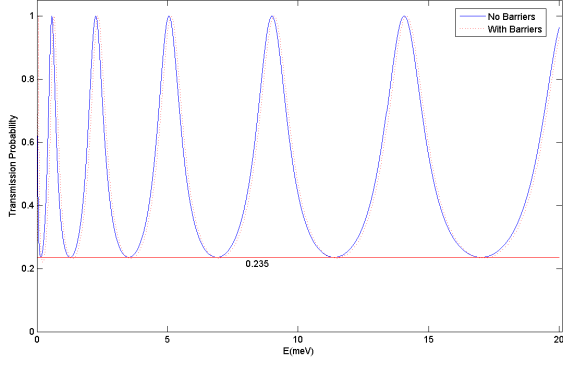


FIG. 8. (Color online) Transmission probability versus incident energy E for the model with the effective mass $m^* = 0.067m_0$ in R_3 , $m^* = m_0$ otherwise, no barriers plotted as solid blue curve, with barriers done as dotted red curve.

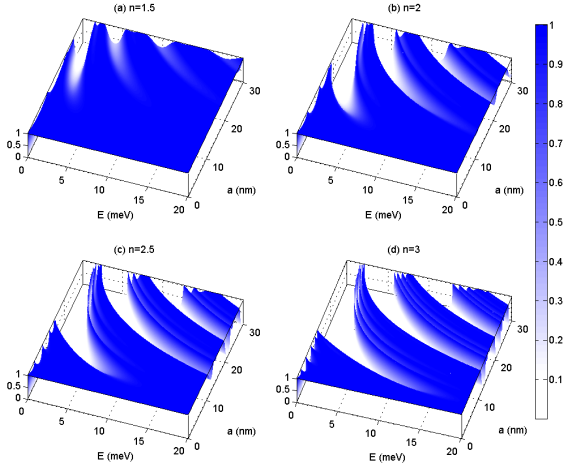


FIG. 9. (Color online) Surface plot of the transmission probability as a function of E and a at (a) $n = 1.5$, (b) $n = 2$, (c) $n = 2.5$ and (d) $n = 3$, with $m^* = 0.067m_0$ for all regions, $V(x) = V_g(x)$ in R_3 and $V(x) = 0\text{meV}$ otherwise.

gaps^{67–71} and resonant tunneling domains^{72–76} appear in the present system shown in Fig. 9. The presence of the transmission gaps is the most fascinating finding in this study. It is readily proved that the widths of the transmission gaps grow with increasing the corrugation amplitude a . The cause is that the larger the distances between adjacent wells in the geometric potential $V_g(x)$, the less the communication or coupling between adjacent wells⁷⁷. As periodical corrugations presented in R_3 , the factor w in Eq. (16) is a function of x as $w = 1/\sqrt{1 + a^2\gamma^2 \sin^2(\gamma x)}$, in R_3 x_j must be replaced by ξ_j

$$\xi_j = \int_0^{x_j} \sqrt{1 + a^2\gamma^2 \sin^2(\gamma x)} dx. \quad (29)$$

According to this integral, the distance between adjacent wells naturally grows with increasing the corrugation am-

plitude. Another aspect of the transmission probability is that the transmission gaps become wider when n is larger with a fixed a , the tunneling domains do narrower correspondingly. The reason is that the more the number of the wells, the stronger their reflections. The resonant tunneling domains are formed essentially by the coupling between adjacent wells, with respect to resonant energy domains^{77,78}. As an application potential, the transmission gaps mean that electron is mostly reflected, but the tunneling domains do that electron can readily pass.

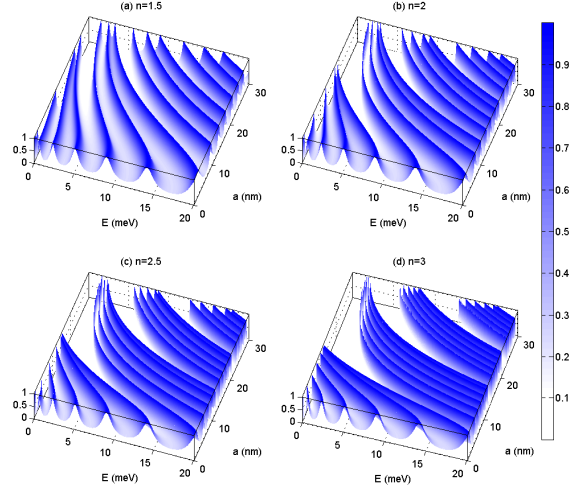


FIG. 10. (Color online) Surface plot of the transmission probability as a function of E and a at (a) $n = 1.5$, (b) $n = 2$, (c) $n = 2.5$ and (d) $n = 3$, with $m^* = 0.067m_0$ in R_3 and $m^* = m_0$ elsewhere, $V(x) = V_g(x)$ in R_3 , $V(x) = 20\text{meV}$ in R_2 and R_4 and $V(x) = 0\text{meV}$ otherwise.

In the considered case, the model with $m^* = 0.067m_0$ in R_3 fabricated by GaAs substrate and $m^* = m_0$ otherwise, with $V(x)$ in Eq. (17), the transmission probability as a function of E and a is described in Fig. 10 for (a) $n = 1.5$, (b) $n = 2$, (c) $n = 2.5$ and (d) $n = 3$. In striking contrast to Fig. 9, Fig. 10 shows that tunneling peaks and valleys evidently occur in the tunneling domains. Significantly, the transmission gaps are still kept. That is to say that the boundaries and the double barriers cannot considerably influence the transmission gaps, but they construct the tunneling peaks and valleys in the tunneling domains, especially when the amplitude a is small. This result can be directly manifested by that the bottom of the valleys is still a certain constant at $a = 0$, which well agrees with that described in Fig. 8. Additionally, it is worthwhile to note that the number of the tunneling peaks in each of the tunneling domains is equivalent to that of the wells in the geometric potential.

In order to highlight the influences of the double barriers and the layer thickness h to the transmission probability, in the case of $n = 3$ and $a = 14\text{nm}$, the transmission probability as a function of E is plotted in Fig. 11. Strikingly, it shows that the transmission gaps are mostly provided by the corrugations. The peaks and valleys in the

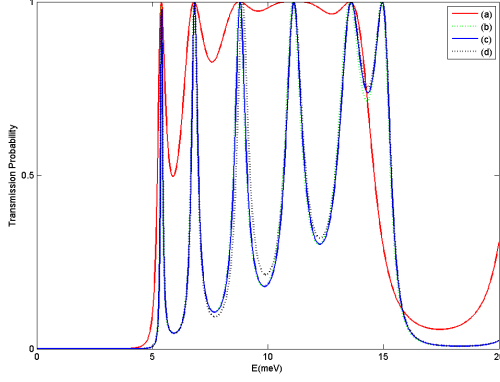


FIG. 11. (Color online) Transmission probability versus E with $n = 3$ and $a = 14\text{nm}$ for (a) $m^* = 0.067m_0$ for all regions, $V(x) = V_g(x)$ in R_3 and $V(x) = 0\text{meV}$ otherwise, (b) $m^* = 0.067m_0$ in R_3 and $m^* = m_0$ otherwise, $V(x) = V_g(x)$ in R_3 and $V(x) = 0\text{meV}$ otherwise, (c) $m^* = 0.067m_0$ in R_3 and $m^* = m_0$ otherwise, $V(x) = V_g(x)$ in R_3 , $V(x) = 20\text{meV}$ in R_2 and R_4 , $V(x) = 0\text{meV}$ otherwise, and (d) $m^* = 0.067m_0$ in R_3 and $m^* = m_0$ otherwise, $V(x) = V'_g(x)$ with $h = 1\text{nm}$ in R_3 , $V(x) = 20\text{meV}$ in R_2 and R_4 , and $V(x) = 0\text{meV}$ otherwise.

tunneling domains are mainly formed by the boundaries between adjacent regions in which electron has different masses. And the boundaries can make the transmission gaps flatter. Trivially, the double barriers and the layer thickness affect on the valleys at a small scale.

V. CONCLUSIONS

A particular component of the considered model is the presence of periodically corrugated thin layer. The corrugated deformation contributes the geometric potential V_g , a sequence attractive potential wells, to the electron across the corrugated layer. The number of wells is determined by the period number n of the corrugations as $2n$. The depth of wells grows with increasing the amplitude a of the corrugations. Approximately, the geometric potential can be roughly equivalent to a sequence square potential wells. The square wells can be structured by

introducing periodically magnetic fields. In terms of the magnetic field, the filter designed for electron with certain energy is the vector-tunable filter⁷⁹. By means of the surface curvature, the filter structured for electron with certain energy can be named as a curvature-tunable filter. When the layer thickness h is considered, the potential V_g should be replaced by V'_g , which includes the modification given by the layer thickness h . For the sake of application, the difference between adjacent wells can be controlled by depositing the layer thickness.

The most fascinating finding in the present study is the presence of the transmission gaps and resonant tunneling domains resulting from the periodic corrugations. In the gaps electron is mostly reflected, in the tunneling domains electron readily passes. Additionally, in the resonant tunneling domains the resonant splitting peaks and valleys essentially attribute to the boundaries between adjacent regions in which electron has different effective masses, and is slightly influenced by the layer thickness h . These results can provide a considerable access for experimenters to fabricate nanoelectronic device. As a potential application, we can control the widths of the transmission gaps by the amplitude a and period number n of the corrugations, design the resonant splitting peaks and valleys by depositing different materials in adjacent regions with certain thickness. Experimentally, the nanocorrugated thin films can be obtained by the detachment method^{1,2}. The corrugated nanofilms fabricated from narrow-gap and gapless semiconductors can be the most promising objects for experiment. In real physical experiments, Coulomb electron interaction, spin-orbital coupling, screening effects and atomic structure need to be considered for two-dimensional curved systems. These interesting questions need to be studied further.

ACKNOWLEDGMENTS

This work is supported by the National Natural Science Foundation of China (under Grant Nos. 11047020, 11404157, 11347126, 11304138, 11275097, 11475085, 11535005).

* Email: wangyl@chenwang.nju.edu.cn

† Email: zonghs@nju.edu.cn

¹ V. Ya. Prinz, D. Grützmacher, A. Beyer, C. David, B. Ketterer, and E. Deckardt 2001 *Nanotechnology* **12** 399

² V. Ya. Prinz, 2006 *Phys. Status Solidi B* **243** 3333

³ X. Li 2008 *J. Phys. D: Appl. Phys.* **41** 193001

⁴ A. M. Turner, V. Vitelli, and D. R. Nelson 2010 *Rev. Mod. Phys.* **82** 1301

⁵ S. V. Mutilin, R. A. Soots, A. B. Vorob'ev, D. G. Ikusov, N. N. Mikhailov, and V. Ya. Prinz 2014 *J. Phys. D: Appl. Phys.* **47** 295301

⁶ Y. Zhang, Z. Yan, K. Nan, D. Xiao, Y. Liu, H. Luan, H. Fu, X. Wang, Q. Yang, J. Wang, W. Ren, H. Si, F. Liu, L. Yang, H. Li, J. Wang, X. Guo, H. Luo, L. Wang, Y. Huang, and A. Rogers 2015 *Pro. Nat. Acad. Sci.* **112** 11757

⁷ O. G. Schmidt and K. Eberl 2001 *Nature* **410** 168

⁸ A. B. Vorob'ev, K.-J. Friedland, H. Kostial, R. Hey, U. Jahn, E. Wiebicke, Ju. S. Yukecheva, and V. Ya. Prinz 2007 *Phys. Rev. B* **75** 205309

⁹ J. Zang, M. Huang, and F. Liu 2007 *Phys. Rev. Lett.* **98** 146102

¹⁰ E. V. Naumova, V. Ya. Prinz, S. V. Golod, V. A. Seleznev, R. A. Soots, and V. V. Kubarev 2009 *J. Opt. A: Pure Appl.*

- Opt.* **11** 074010
- ¹¹ P. Froeter, X. Yu, W. Huang, F. Du, M. Li, I. Chun, S. H. Kim, K. J. Hsia, J. A. Rogers, and X. Li 2013 *Nanotechnology* **24** 475301
 - ¹² M. H. T. Dastjerdi, M. Djavid, and Z. Mi 2015 *Appl. Phys. Lett.* **106** 021114
 - ¹³ S. Tanda, T. Tsuneta, Y. Okajima, K. Inagaki, K. Yamaya, and N. Hatakenaka 2002 *Nature* **417** 397
 - ¹⁴ Z. S. Yoon, A. Osuka, and D. Kim 2009 *Nature Chem.* **1** 113
 - ¹⁵ P. Monceau 2012 *Adv. Phys.* **61** 325
 - ¹⁶ J. Onoe, T. Nakayama, M. Aono, and T. Hara 2003 *Appl. Phys. Lett.* **82** 595
 - ¹⁷ J. Onoe, T. Ito, S.-I. Kimura, K. Ohno, Y. Noguchi, and S. Ueda 2007 *Phys. Rev. B* **75** 233410
 - ¹⁸ Y. Toda, S. Ryuzaki, and J. Onoe 2008 *Appl. Phys. Lett.* **92** 094102
 - ¹⁹ J. Onoe, T. Ito, H. Shima, H. Yoshioka, and S.-I. Kimura 2012 *Europhys. Lett.* **98** 27001
 - ²⁰ H. Masuda, J. Onoe, and H. Yasuda 2015 *Carbon* **81** 842
 - ²¹ G. Ferrari, and G. Cuoghi 2008 *Phys. Rev. Lett.* **100** 230403
 - ²² B. Jensen, and R. Dandoloff 2009 *Phys. Rev. A* **80** 052109
 - ²³ C. Ortix, and J. van den Brink 2011 *Phys. Rev. B* **83** 113406
 - ²⁴ Y.-L. Wang, L. Du, C.-T. Xu, X.-J. Liu, and H.-S. Zong 2014 *Phys. Rev. A* **90** 042117
 - ²⁵ H. Jensen, and H. Koppe 1971 *Ann. Phys. (N.Y.)* **63** 586
 - ²⁶ R. C. T. da Costa 1981 *Phys. Rev. A* **23** 1982
 - ²⁷ R. C. T. da Costa 1982 *Phys. Rev. A* **25** 2893
 - ²⁸ Y.-L. Wang, and H.-S. Zong 2016 *Ann. Phys. (N.Y.)* **364** 68
 - ²⁹ H. Aoki, M. Koshino, D. Takeda, H. Morise, and K. Kuroki 2001 *Phys. Rev. B* **65** 035102
 - ³⁰ N. Fujita and O. Terasaki 2005 *Phys. Rev. B* **72** 085459
 - ³¹ M. Koshino and H. Aoki 2005 *Phys. Rev. B* **71** 073405
 - ³² J. Goldstone and R. L. Jaffe 1992 *Phys. Rev. B* **45** 14100
 - ³³ G. Cantele, D. Ninno, and G. Iadonisi 2000 *Phys. Rev. B* **61** 13730
 - ³⁴ M. Encinosa and L. Mott 2003 *Phys. Rev. A* **68** 014102
 - ³⁵ H. Taira and H. Shima 2007 *J. Phys.: Conf. Ser.* **61** 1142
 - ³⁶ H. Taira and H. Shima 2007 *Surf. Sci.* **601** 5270
 - ³⁷ B. Jensen 2009 *Phys. Rev. A* **80** 022101
 - ³⁸ C. Ortix and J. van den Brink 2010 *Phys. Rev. B* **81** 165419
 - ³⁹ A. Marchi, S. Reggiani, M. Rudan, and A. Bertoni 2005 *Phys. Rev. B* **72** 035403
 - ⁴⁰ E. Zhang, S. Zhang, and Q. Wang 2007 *Phys. Rev. B* **75** 085308
 - ⁴¹ G. Cuoghi, G. Ferrari, and A. Bertoni 2009 *Phys. Rev. B* **79** 073410
 - ⁴² H. Shima, H. Yoshioka, and J. Onoe 2009 *Phys. Rev. B* **79** 201401(R)
 - ⁴³ A. Szameit, F. Dreisow, M. Heinrich, R. Keil, S. Nolte, A. Tünnermann, and S. Longhi 2010 *Phys. Rev. Lett.* **104** 150403
 - ⁴⁴ J. Kim, V. Chua, G. A. Fiete, H. Nam, A. H. MacDonald, and C.-K. Shih 2012 *Nature Phys.* **8** 464
 - ⁴⁵ L. L. Chang and L. Esaki 1992 *Phys. Today* **45**(10) 36
 - ⁴⁶ F. A. Buot 1993 *Phys. Rep.* **234** 73
 - ⁴⁷ M. S. Kushwaha, P. Halevi, G. Martínez, L. Dobrzynski, and B. Djafari-Rouhani 1994 *Phys. Rev. B* **49** 2313
 - ⁴⁸ C. Lamberti 2004 *Surf. Sci. Rep.* **53** 1
 - ⁴⁹ X.-W. Jiang, S.-S. Li, and L.-W. Wang 2012 *Solid-State Electron* **68** 56
 - ⁵⁰ S. Xu, Z. Yan, K.-I. Jang, W. Huang, H. Fu, J. Kim, Z. Wei, M. Flavin, J. McCracken, R. Wang, A. Badea, Y. Liu, D. Xiao, G. Zhou, J. Lee, H. U. Chung, H. Cheng, W. Ren, A. Banks, X. Li, U. Paik, R. G. Nuzzo, Y. Huang, Y. Zhang, and J. A. Rogers 2015 *Science* **347** 154
 - ⁵¹ M. Encinosa 2000 *IEEE Trans. Electron Devices* **47** 878
 - ⁵² S. Ono and H. Shima 2009 *Phys. Rev. B* **79** 235407
 - ⁵³ S. Ono and H. Shima 2010 *Physica E* **42** 1224
 - ⁵⁴ H. Taira and H. Shima 2010 *J. Phys.: Condens. Matter* **22** 075301
 - ⁵⁵ H. Shima 2012 *Phys. Rev. B* **86** 035415
 - ⁵⁶ M. Blencowe 2004 *Phys. Rep.* **395** 159
 - ⁵⁷ A. V. Chaplik and R. H. Blick 2004 *New J. Phys.* **6** 33
 - ⁵⁸ Z.-L. Xiang, S. Ashhab, J. Q. You, and F. Nori 2013 *Rev. Mod. Phys.* **85** 623
 - ⁵⁹ R. Amalraj and S. Sambandan 2014 *J. Appl. Phys.* **116** 164507
 - ⁶⁰ Y. P. Li, A. Zaslavsky, D. C. Tsui, M. Santos, and M. Shayegan 1990 *Phys. Rev. B* **41** 8388
 - ⁶¹ L. Y. Chen and C. S. Ting 1991 *Phys. Rev. B* **43** 4534
 - ⁶² L. Y. Chen and C. S. Ting 1991 *Phys. Rev. B* **43** 2097
 - ⁶³ C. L. Kane and M. P. A. Fisher 1992 *Phys. Rev. B* **46** 15233
 - ⁶⁴ C. R. Doering and J. C. Gadoua 1992 *Phys. Rev. Lett.* **69** 2318
 - ⁶⁵ H. S. Nguyen, D. Vishnevsky, C. Sturm, D. Tanese, D. Solnyshkov, E. Galopin, A. Lemaitre, I. Sagnes, A. Amo, G. Malpuech, and J. Bloch 2013 *Phys. Rev. Lett.* **110** 236601
 - ⁶⁶ Y. Ando and T. Itoh 1987 *J. Appl. Phys.* **61** 1497
 - ⁶⁷ A. Khelif, B. Djafari-Rouhani, J. O. Vasseur, and P. A. Deymier 2003 *Phys. Rev. B* **68** 024302
 - ⁶⁸ X. Chen, L.-G. Wang, and C.-F. Li 2009 *Phys. Rev. A* **80** 043839
 - ⁶⁹ X. Chen and J.-W. Tao 2009 *Appl. Phys. Lett.* **94** 262102
 - ⁷⁰ W.-T. Lu, S.-J. Wang, W. Li, Y.-L. Wang, and H. Jiang 2012 *Physica B* **407** 918
 - ⁷¹ Y. Xu, Y. He, and Y. Yang 2015 *Physica B* **457** 188
 - ⁷² X.-W. Liu and A. P. Stamp 1993 *Phys. Rev. B* **47** 16605
 - ⁷³ Y. Guo, B.-L. Gu, Z.-Q. Li, J.-Z. Yu, and Y. Kawazoe 1998 *J. Appl. Phys.* **83** 4545
 - ⁷⁴ Z. Y. Zeng, L. D. Zhang, X. H. Yan, and J. Q. You 1999 *Phys. Rev. B* **60** 1515
 - ⁷⁵ Y. Xu, Y. He, and Y. Yang 2014 *Appl. Phys. A* **115** 721
 - ⁷⁶ C. H. Pham and V. L. Nguyen 2015 *J. Phys.: Condens. Matter* **27** 095302
 - ⁷⁷ X.-W. Liu and A. P. Stamp 1994 *Phys. Rev. B* **50** 1588
 - ⁷⁸ W.-T. Lu, W. Li, Y.-L. Wang, H. Jiang, and C.-T. Xu 2013 *Appl. Phys. Lett.* **103** 062108
 - ⁷⁹ L. Dell'Anna and A. De Martino 2009 *Phys. Rev. B* **80** 155416